Infection dynamics and virulence potential of clinical *Pseudomonas aeruginosa* isolates in a human airway epithelium model system

Claudia Antonella Colque[1,#,*], Signe Lolle[1,#], Ruggero La Rosa[1,*], Maria Pals Bendixen[1], Filipa Bica Simões[1], Kasper Aanæs[2,3], Søren Molin[4], Helle Krogh Johansen[1,2*].

[1] Department of Clinical Microbiology 9301, Rigshospitalet, 2100 Copenhagen Ø, Denmark

[2] Department of Clinical Medicine, Faculty of Health and Medical Sciences, University of Copenhagen, 2200 Copenhagen, Denmark.

[3] Department of Otorhinolaryngology, Head and Neck Surgery & Audiology, Rigshospitalet, 2100 Copenhagen Ø, Denmark.

[4] The Novo Nordisk Foundation Center for Biosustainability, Technical University of Denmark, 2800 Kgs. Lyngby, Denmark.

# These authors contributed equally.

* Corresponding authors: Claudia Antonella Colque (antcol@biosustain.dtu.dk), Ruggero La Rosa (rugros@dtu.dk), Helle Krogh Johansen (hkj@biosustain.dtu.dk).

Abstract

Persistent bacterial infections constitute an increasing health problem, which is often associated with antibiotic resistance. However, investigations of chronic lung inflammation and persistent infections with *Pseudomonas aeruginosa* in people with cystic fibrosis (pwCF) show that treatment failures may instead be rooted in host-microbe interactions developing after bacterial colonization of the CF airways. Using a laboratory infection model based on human airway epithelial tissues, cultured in an Air-Liquid Interface (ALI) system, we simulated the infection process of various *P. aeruginosa* strains to investigate the colonisation dynamics and the virulence potential during infection of nasal epithelial cultures from both non-CF and CF donors in addition to an immortalized bronchial cell line, BCi-NS1.1. Infections by *P. aeruginosa* reference strains and clinical isolates from pwCF were employed. While reference and patients' early strains exhibited high virulence and increased epithelial disruption, clinically adapted strains showed reduced virulence potential and limited epithelial damage regardless of the host cell type or clonal lineage. Dual RNA-seq analysis revealed that colonization of ALI cultures with virulent PAO1 significantly upregulated inflammatory pathways in host cells, an effect that was dampened in the less virulent *pscC* mutant strain lacking the type III secretion system. Simultaneously, while bacterial gene expression was similar in wild-type and BCi-NS1.1 cultures, in CF cells, the *pscC* strain showed dysregulation of genes involved in iron starvation, respiration, and quorum sensing pathways. Altogether, our results summarize the infection dynamics in the ALI model system and in pwCF, and provide a snapshot of the interplay between the airway epithelium and *P. aeruginosa*.

Introduction

With increasing lifespans and changes in lifestyle, persistent bacterial infections are on the rise [1]. Although antibiotics are generally effective, diagnosing and treating these infections is often challenging because of their complexity and the continuous changes in both the host and pathogen [2]. This is worsened by the lack of robust and reliable model systems to predict infection outcomes and treatment efficacy. However, by understanding treatment failures in relevant model systems, better diagnostics and therapies can be developed.

People with cystic fibrosis (pwCF) often suffer from persistent bacterial infections caused by a plethora of bacterial pathogens that colonize the airways and persist for decades. CF is caused by mutations in the cystic fibrosis transmembrane conductance regulator protein (CFTR), which is crucial for fluid homeostasis [3]. CFTR mutations result in impaired chloride secretion, increased mucus viscosity and reduced cilia beating, ultimately leading to mucociliary clearance [4]. This creates the perfect environment for pathogenic bacteria, such as *Pseudomonas aeruginosa*, which is the leading cause of respiratory morbidity and mortality in pwCF [5,6]. Recent advances in CFTR modulator therapies, particularly elexacaftor/tezacaftor/ivacaftor (ETI), significantly improve clinical well-being in pwCF by correcting and potentiating the function of the CFTR channels [7]. In addition, decreases in bacterial pathogen counts during ETI treatment have been shown [8]. However, *P. aeruginosa* persists in most patients, indicating the need for a deeper understanding of the relationship between ETI treatment and *P. aeruginosa* infections in pwCF [9–11].

Early infections are caused by environmental *P. aeruginosa* strains which adapt, over the years, to the CF environment through genetic, metabolic, and phenotypic changes [12,13]. This enhances antibiotic resistance, immune system evasion and a biofilm lifestyle and reduces virulence factor production [14–17]. In most patients, the initial clone drives within-host adaptation. Person-to-person transmission has also been documented in pwCF, and especially *P. aeruginosa* clones such as the DK01 and DK02 (Denmark), and high-frequent clones such as the C clone (ST17 clone, present in Europe and North America and persistent in pwCF) and PA14 (ST253 clone, found worldwide with affinity to CF and non-CF infections) have this capability [18–24]. However, how colonization and infection dynamics evolve during infection from a *P. aeruginosa*-human airway point of view remains largely unclear. This includes 1) the role of virulence factors, toxins, and specific dominant strains in tissue invasion and immune escape, 2) the epithelial responses and long-term effects on epithelial integrity and function,

and 3) how modulator treatment changes the infection pattern and the interaction between the airway epithelium and the pathogen. Understanding the early stages of colonization, therefore, may shed light on the bacterial pathogenic potential, antibiotic treatment failure, and allow exploration of new treatment options. In addition, the lack of reliable *in vitro* model systems which recreate the infectious microenvironment for studying infection processes in the airway limits our understanding of colonization dynamics and bacterial virulence potential within human tissue [25].

Various model systems including immortalized cell lines, primary cells, tissue explants, and animal models have been created to study *P. aeruginosa*-human airway interactions [26]. 3D air-liquid interface (ALI) airway tissue cultures closely mimic the human airway epithelium, exhibiting differentiation, cell polarity, mucus production, and ciliary beating, which are fundamental for understanding infection dynamics and colonization processes [27,28]. Nevertheless, only few studies have used ALI systems to shed light on bacterial infection processes, resistance mechanisms and metabolic adaptation [16,29–34]. However, these studies have used laboratory strains which do not reflect the complexity of clinical CF isolates and their infection dynamics.

In this study, we used ALI cultures to profile *P. aeruginosa* infection using 12 clinical strains from frequent and distinct lineages and compared them with standard reference strains. We determined the overall physiological tissue response to the bacterial infections, such as epithelial integrity, cytotoxicity, cytokine secretion, and bacterial colonization patterns in infections of primary non-CF and CF nasal epithelial cells, and the bronchial cell line BCi-NS1.1, as well as the impacts of the CFTR modulator, ETI. Dual RNA-seq revealed host and bacterial response at the molecular level, unfolding their interactions. Our results investigate early infection stages of airway epithelium and highlight the importance of host-pathogen model systems to understand infection dynamics and develop new advanced therapies.

Results

Host responses upon bacterial infections in ALI airway culture models

To study the early dynamics of epithelial colonization, and to determine whether epithelial tissues from different hosts exhibit individual responses upon *P. aeruginosa* infections, we performed bacterial infection assays using a model system of airway epithelial cells grown under ALI conditions (Fig S1). Specifically, we evaluated infection capabilities and epithelial

responses, using differentiated primary nasal cells from pwCF (n = 7) and non-CF (n = 3) donors along with the human non-smoker immortalized bronchial BCi-NS1.1 cell line [35] infected with a panel of *P. aeruginosa* strains (Fig S1, Table S1). Specifically for each infection, we quantified bacterial proliferation and epithelium responses by measuring: 1) the transepithelial electrical resistance (TEER) to quantify the integrity and permeability of the epithelium, 2) the release of lactate dehydrogenase (LDH) in the basolateral media to quantify the induced epithelial cell lysis, 3) the secretion of the chemokine Interleukin-8 (IL-8) to quantify the onset of inflammation, and 4) the bacterial colony-forming units (CFU) (Table S2: Infection dynamics). Infections were carried out using a collection of early (*_E), intermediate (*_I) and late (*_L) clinical isolates from pwCF belonging to distinct clone types (lineages which differ by >10,000 SNPs), which comprise different stages of CF adaptation, evolutionary histories and infection scenarios [36,37]. These clone types were chosen based on their frequency in the Copenhagen CF Clinic (DK01 and DK02) and worldwide (C and PA14 clone, DK06 and DK19 clones in Denmark, respectively). In addition, we included standard *P. aeruginosa* reference strains (PAO1 and PA14), including a PAO1 derivative lacking the virulence determinant T3SS (*pscC*), which is involved in host colonization, invasion and cell damage [32] (Table S1). It has been shown that the Type III secretion plays an important role in the transition from acute to chronic/persistent infection occurring during host adaptive evolution [38,39]. The chosen bacteria exhibit distinct phenotypes, with laboratory and early strains characterized by high growth rates and motility, whereas intermediate and late strains were characterized by slower growth, reduced motility and mild-to-high increased minimum inhibitory concentration (MIC) to tobramycin, ciprofloxacin and ceftazidime (Fig S2). To account for the varying growth rates among strains (Fig S2C) and to ensure a comparable bacterial count at the end of the infections regardless of strain or cell type, infections were conducted for 14 h for laboratory, early, and intermediate strains, and for 38 h for late strains (DK01_L, DK02_L, DK06_L, and DK19_L). All infection data are detailed in Table S2.

Consistent with the experimental set-up, no significant differences in CFUs were observed across bacterial strains and ALI models on the apical (non-attached) side, as well as the combined CFUs (total CFU) from all ALI compartments (Kruskal-Wallis followed by Dunn's post-hoc test, $p>0.05$) (Fig S3). Additionally, Pearson's correlation analysis showed no significant correlation between the total CFU relative to TEER drop (r=-0.27, p=0.0010), LDH release (r=-0.004, p=0.9601), and IL-8 secretion (r=0.12, p=0.1441), indicating independence

of the variables. In addition, strain-specific bacterial infection outcomes (TEER drop, compartment distribution, LDH release and IL-8 secretion) were generally comparable across BCi-NS1.1, non-CF and CF models (Kruskal-Wallis followed by Dunn's post-hoc test, $p>0.05$), except for DK01_L, DK06_L and DK19_L infections, where LDH released in CF was significantly higher compared to non-CF models (Kruskal-Wallis followed by Dunn's post-hoc test, $p<0.01$, Table S2: Infection Dynamics). In all cases, Pearson correlation analysis of infection data across the different ALI models showed values > 0.9 ($p<0.001$) (Fig 1A). This suggests that in our model system, the infection outcomes are mostly dependent on the specific virulence potential of the infecting bacteria rather than conditional to the origin of the host sample.

When comparing across all infections (ALI, n = 194) to increase statistical power, the TEER measurements at time 0 prior to each infection revealed tissue dependent values, with BCi-NS1.1 cultures exhibiting the highest TEER followed by CF and non-CF primary cultures (Kruskal-Wallis followed by Dunn's post-hoc test, $p<0.0001$) (Fig 1B). Similarly, CF cultures exhibited the highest level of cellular damage (LDH release) and highest inflammatory response (IL-8 secretion) (Kruskal-Wallis followed by Dunn's post-hoc test, $p<0.01$) (Fig 1C, D). Comparable results were obtained when discriminating by the duration of infection (14 h vs 38 h) and control treatment (mock) (Fig S4). Moreover, CF cultures exhibited a time-dependent increase of LDH release, underlining the intrinsic fragility of this tissue culture (Kruskal-Wallis followed by Dunn's post-hoc test, $p<0.01$) (Fig S4D).

Next, we evaluated whether ETI treatment altered *P. aeruginosa* infection patterns in the ALI system using primary cells from pwCF and non-CF controls (Table S2: ETI treatment). As expected, 24 hours of ETI treatment resulted in a significant decrease in TEER (paired two-sided t-test, $p<0.0001$) and an increase in transepithelial electrical conductance (TEEC) in CF cells (paired two-sided t-test, $p<0.01$), indicating a treatment response (Fig 2A, B). No effect was observed in non-CF cells (Fig S5C, D). This was confirmed by immunofluorescence staining of the CFTR protein, allowing for a comparison between the ETI-treated and untreated ALI cultures (Fig 2E). Infection outcomes in ETI-treated and untreated ALI cultures after 14h or 38h of infection using the PAO1 laboratory strain and the DK01_I and DK02_L clinical strains showed no differences in TEER, bacterial growth or compartmental distribution of bacteria when comparing different strains, ALI models, or ETI-treatment (Fig 2C, D and Fig S5).

These results suggest that in our ALI system, early infection dynamics are independent of the cell type or treatment and may depend on other factors such as the specific bacterial

lineage, activation of the immune system, antibiotic treatments or change in mucus composition, viscosity, and/or clearance which are currently not possible to recreate in the ALI infection model system used. However, intrinsic differences between host cells such as LDH release and IL-8 secretion, should be considered based on the specific requirements.

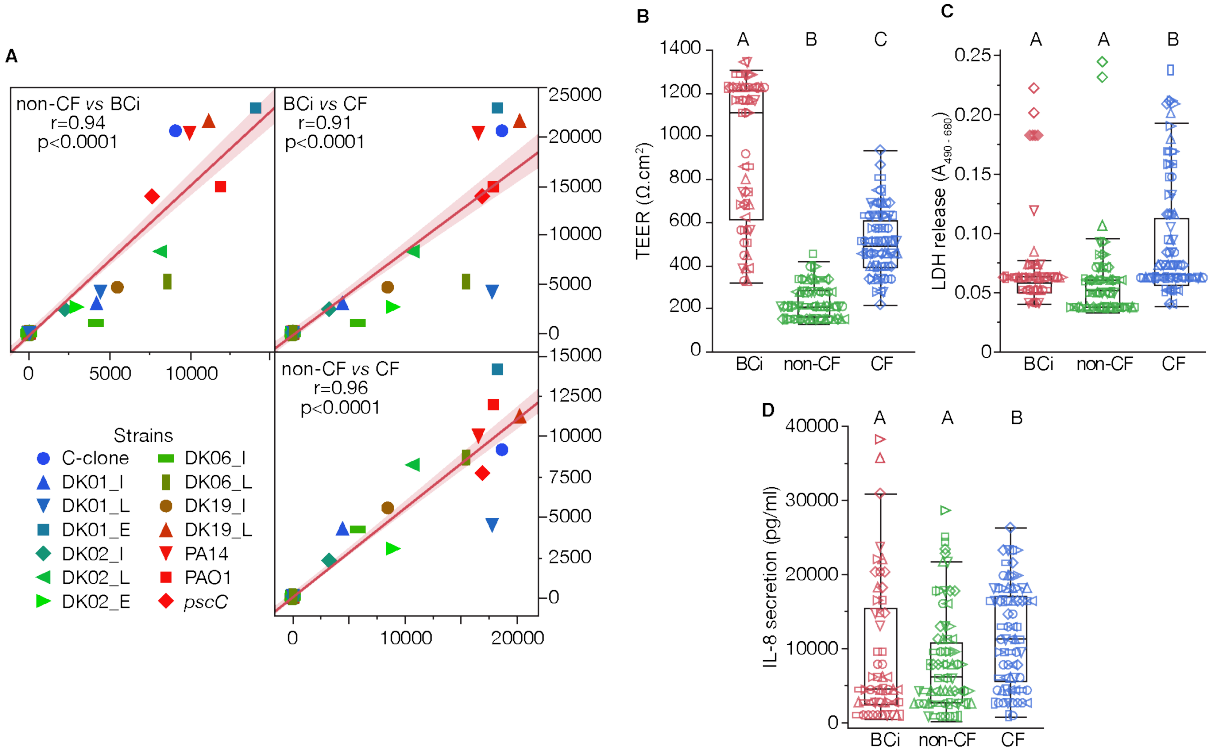

Fig 1. Infection outcomes across ALI tissue types and bacterial strains. A) Pearson correlation analysis of the infection data across cultures and bacterial strains. Pearson's correlation coefficient r, statistical significance (p value), linear fitting between the variables and 95% confidence interval are indicated in the graph. B) TEER measurements of BCi-NS1.1, non-CF and CF cultures after 28 days of differentiation in absence of bacterial infections. C) LDH release by BCi-NS1.1, non-CF and CF airway cultures after 14 or 38 h of infections indicating cytotoxicity post infection. D) IL-8 secretion in the basolateral media by BCi-NS1.1, non-CF and CF cultures 14 or 38 hours post infection indicating a state of inflammation. Infections were carried out at 14 h for early and intermediate strains of DK01, DK02, DK06 and DK19 and laboratory strains PAO1 and PA14 and 38 h for late strains of DK01, DK02, DK06 and DK19. In B, C and D, statistical significance was computed by Kruskal-Wallis followed by Dunn's post-hoc test, where connecting letters report significance between groups ($p<0.05$). CF: cystic

fibrosis; BCi: BCi-NS1.1; TEER: transepithelial electrical resistance; LDH: lactate dehydrogenase; IL-8: interleukin 8.

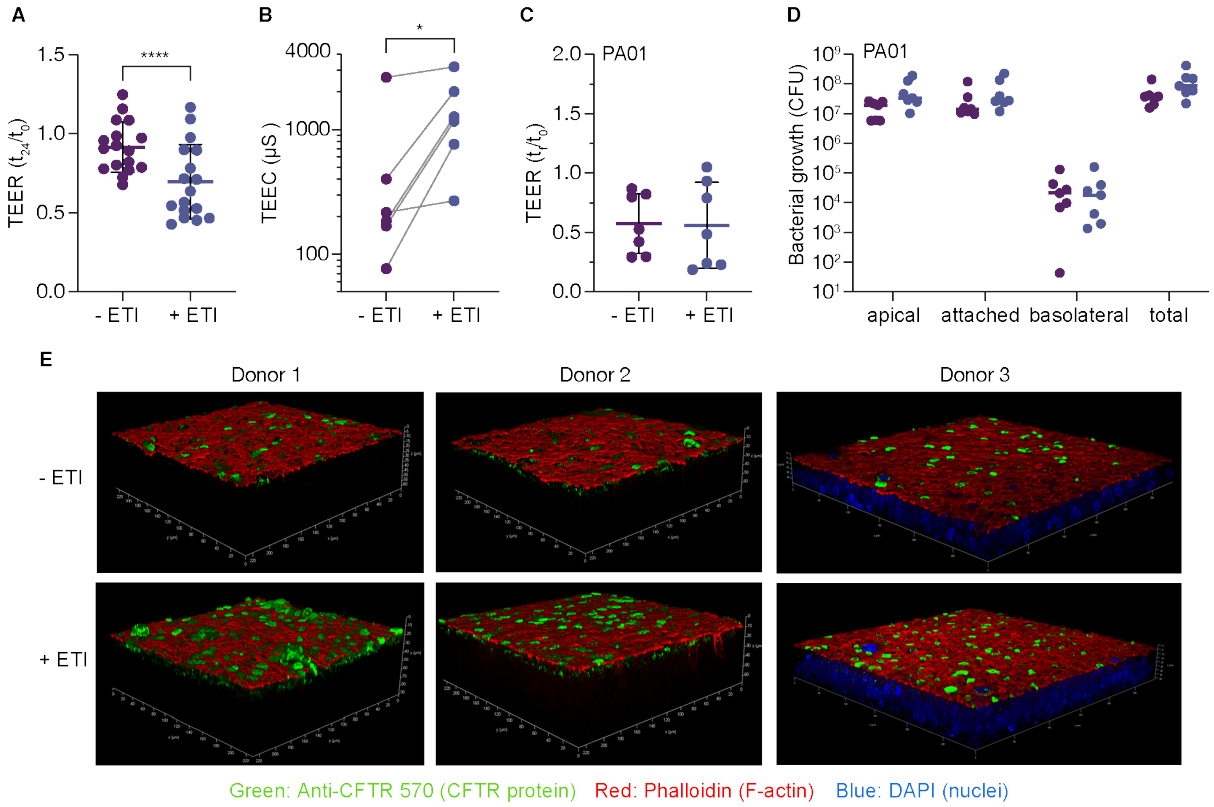

Fig 2. Effect of elexacaftor/tezacaftor/ivacaftor (ETI) treatment on cystic fibrosis transmembrane conductance protein (CFTR) function and infection pattern in cystic fibrosis (CF) cultures**.** A) Fold change in TEER measurements after 24 hours of ETI treatement (+ ETI) or no treatement (- ETI) in ALI cultures from three CF donors homozygous for ΔF508 mutation. B) TEEC after CFTR stimulation in treated (+ ETI) and untreated (- ETI) cells. Each dot represents one independent donor. C) TEER change after 14 h of infection with PAO1 laboratory strain in treated (+ ETI) and untreated (- ETI). D) Bacterial growth (CFU) after 14 h of infection in the apical (non attached / free bacteria), attached to the epithelium, and basolateral compartment, along with the total number of bacteria. In A,C-D, each dot represents one independent experiment and the mean ± SD is included. Statistical significance was calculated by paired two-sided t-test where **p<0.01 and ****p<0.0001. E) Three-dimensional reconstruction of confocal microscopy images of immunofluorescent staining of CFTR protein in ALI cultures from the CF donors treated (+ ETI) and untreated (- ETI). Green: Anti-CFTR 570 (CFTR protein), Red: Phalloidin (F-actin), Blue: DAPI (nuclei). ALI: air-liquid interface; TEER:

transepithelial electrical resistance; TEEC: transepithelial electrical conductance; CFU: colony-forming units.

Strain-specific infection phenotypes of P. aeruginosa

After years of adaptive evolution in pwCF, *P. aeruginosa* changes its phenotype in response to the host environment, including its stresses (e.g. antibiotics, ROS) and host components (e.g. immune cells) [23,40]. Therefore, we aimed to evaluate if differences in strain adaptive evolution and historical contingency restricted the infection capabilities in a convergent manner. Given that bacterial infections progressed similarly across the different cell lines or ETI treatment, for each strain, we averaged by their median the infection data in BCi-NS1.1, non-CF and CF cultures (Table S2: Infection dynamics Avg.).

PCA and K-Means clustering identified four clusters of strains with similar infection properties which can be associated with their virulence and evolutionary stage (Fig 3A). Clusters 1 and 2 correspond to mostly virulent strains characterized by a substantial drop in TEER, increased cytotoxicity (LDH release) and inflammation (IL-8). Contrarily, strains in clusters 3 and 4 show a TEER close to the mock samples, which suggests reduced virulence (Fig 3A, B). Therefore, PC 1 (50% of the variance), clusters strains based on their virulence potential (defined as changes in TEER, LDH and IL-8 variables), while PC 2 (36.2% of the variance) separates strains based on their ability to penetrate the epithelium. Strains from cluster 1, indeed, even at a very low percentage, are found in the basolateral compartment of the ALI cultures, indicating increased penetration through the epithelial layer. Strains from cluster 3 are, instead, found at a lower percentage non-attached/free on the apical side and preferentially attached to the cells either apically or internally (Fig 3). It is worth noting that while the recombinant strain *pscC* and the DK02_L isolate were grouped in cluster 1 and cluster 2, respectively, they show intermediate infection capabilities such as intermediate TEER drop and relatively low LDH and IL-8 release as in clusters 3 and 4 (Fig 3B).

Interestingly, confocal microscopy analyses revealed more features of the infection phenotype: while virulent strains from cluster 1 and 2 colonized the epithelia as large aggregates/biofilm structures, less virulent strains from cluster 3 and 4 infected as single colonies or small bacterial aggregates (Fig 3C and Fig S6). Virulent strains caused cell shredding from the apical side of the epithelia and were found within the epithelial layer as shown by the PA14 strain (Fig 3C). However, variation in colonization phenotype was observed within

each cluster (Fig S6), which could be attributable to the genetic background of each strain. Interestingly, DK01_I and DK02_I strains from cluster 4 were the only bacteria targeting mucus-producing cells (as shown by bacteria overlapping with MUC5AC+ cells) (Fig 3C and Fig S6).

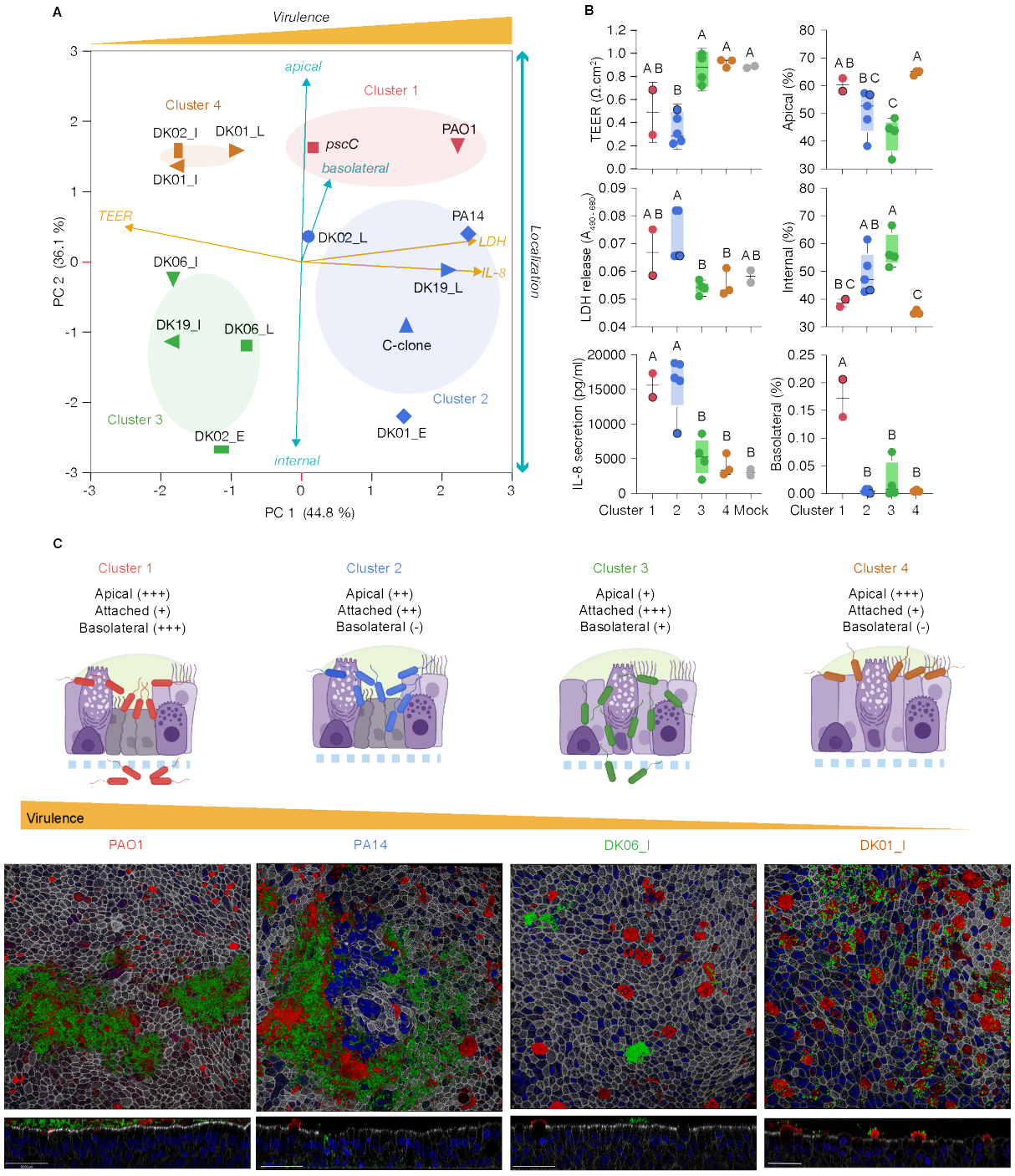

Fig 3. Infection phenotypes of *Pseudomonas aeruginosa* strains. A) PCA and K-mean clustering of the infection phenotypes of laboratory (PAO1, *pscC*, PA14 and C-clone) and

clinical strains (early, intermediate, and late DK01, DK02, DK06 and DK19) of *P. aeruginosa.* Each symbol represents the median infection phenotypes in BCi-NS1.1, non-CF and CF cultures explained by the variables TEER, LDH release, IL-8 secretion, and distribution of bacteria in the apical, attached, and basolateral compartment. K-mean clusters (1 to 4) and PCA loadings are colour-coded to underline groupings of strains and explained variance, respectively. B) Box plot of the specific K-mean clusters characteristics for TEER, LDH release, IL-8 secretion, and normalized distribution of CFUs in the apical, attached and basolateral compartment. The outlined symbols in clusters 1 and 2 represent strains *pscC* and DK02_L, respectively. Statistical significance was computed by Kruskal-Wallis followed by Dunn's post-hoc test, connecting letters report significance between groups ($p<0.05$). C) Colonization phenotype of strain-specific clusters in CF cells. Schematic representation of ALI-CF epitheliums (purple) challenged with strains from clusters 1 (red), 2 (blue), 3 (green), and 4 (brown). Representative confocal microscopy images of CF-ALI cultures infected with strains from Cluster 1 (PAO1), Cluster 2 (PA14), Cluster 3 (DK06_I) and Cluster 4 (DK01_I). Top and side views of transwells are shown. Representative images from all strains infecting CF-ALI cultures are shown in Fig S6. Immunofluorescence staining: sGFP (green) staining chromosomally tagged bacteria; MUC5AC (red) specific for mucus producing cells; Phalloidin (white) specific for actin and DAPI (blue) nuclear stain. Staining's were done in three biological replicates, one representative image is shown for each infection. PCA: principal component analysis; TEER: transepithelial electrical resistance; LDH: lactate dehydrogenase; IL-8: interleukin 8.

Dual RNA-sequencing of P. aeruginosa *infecting ALI cell cultures*

While different bacterial strains showed similar infection patterns regardless of the infected ALI culture, the molecular responses of both the bacteria and the host might be strongly influenced by the specific cell culture and bacterial strain combination. To test this hypothesis, we performed dual RNA-seq experiments of ALI cultures from a CF and a non-CF donor and the BCi-NS1.1 cell line, infected with PAO1, *pscC* strain and mock (Fig 4A, Table S2: RNAseq). This approach allowed us to analyze the molecular response of bacteria with a clean background, eliminating the variable of the historical contingency of clinical strains, while still capturing the colonization process of highly virulent (PAO1) and intermediate virulent-like (*pscC*) clinical strains (Fig 3A).

PCA analysis of the host expression response (18746 genes, Fig 4B) showed that: 1) the transcriptional program of host-infected tissues (ALI-PAO1 and ALI-*pscC*) differed from that of non-infected cultures (ALI-mock) on PC 1 (Fig 4B), and 2) primary cells (non-CF and CF) exhibited different host responses relative to the BCi-NS1.1 cell line on PC 2 (Fig 4B). Meanwhile, the analysis of the bacterial expression profiles (4255 genes, Fig 4C) revealed subclusters based on: 1) the ALI model with non-CF and BCi-NS1.1 colocalizing on PC 1 (Fig 4C), and 2) the bacterial genetic background (top *pscC*, bottom PAO1) on PC 2 (Fig 4C). Bacteria colonizing non-CF and the BCi-NS1.1 ALI models showed almost identical gene expression profiles independently of the strain used (PAO1 or *pscC*), while growth on CF airway tissue seemed to drive a distinct bacterial expression profile. As a control and to validate our RNA-seq experiment, we correlated the IL-8 secretion during the infection with its corresponding gene (CXCL8) expression (Fig 4D), which showed a positive and significant correlation (Pearson's r= 0.9891; p < 0.0001). This confirms that infected samples have higher cytokine levels compared to the mock indicating ongoing inflammation.

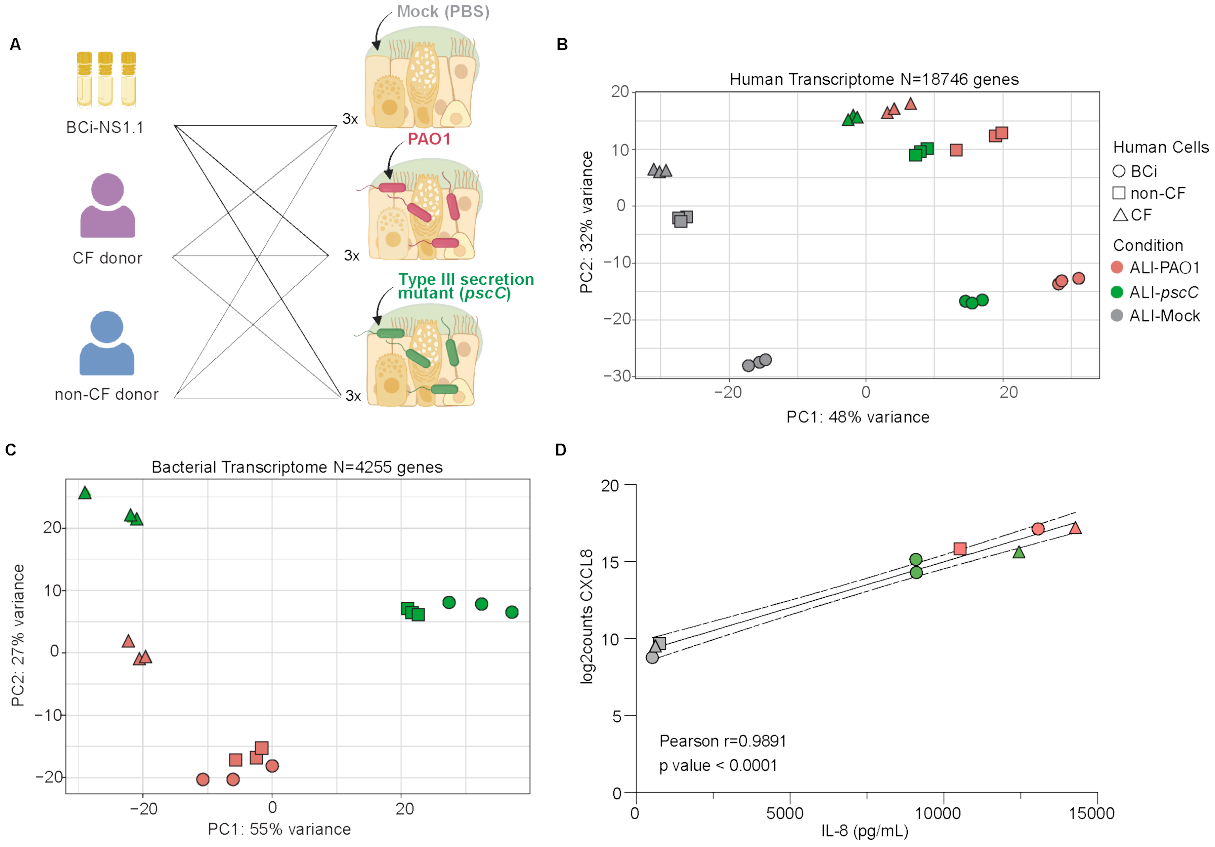

Fig 4. Exploring the transcriptional responses from human and pathogen upon co-culture. A) Schematic representation of the ALI cultures, host tissues (CF, purple; non-CF, blue; BCi-

NS1.1, yellow) and bacteria (PAO1, red; *pscC*, green) used to perform infections and subsequent dual-RNAseq. RNA was extracted from three (3x) biological replicates. PCA of log_2 read counts from B) the host and C) the pathogen. Data included the reads of 18746 genes from the human transcriptome and 4255 from the *Pseudomonas aeruginosa* transcriptome, from which differential gene expression analysis was performed. Human tissues are presented by symbol shapes: BCi-NS1.1 (circle), CF (triangle) and non-CF (square). Non infected (mock) cultures are colored in grey, whereas ALI cultures with PAO1 or *pscC* are shown in red and green, respectively. Each dot represents one biological replicate. D) Regression lines and Pearson correlation coefficient for IL-8 quantification and the gene expression (log_2 read counts). 95% confidence interval lines for the linear regression fit are included. ALI: air-liquid interface; CF: cystic fibrosis; PCA: Principal component analysis; TEER: transepithelial electrical resistance; IL-8: interleukin 8.

Cellular and inflammatory responses in ALI cultures upon infection with PAO1 and pscC

To characterize the molecular basis of the host response with either PAO1 or *pscC*, we performed individual differentially expressed genes (DEG) comparisons between a) PAO1-infected and mock cultures (Fig 5A), and b) PAO1-infected and *pscC*-infected cells (Fig 5D). For each comparison, we first compared gene convergence/divergence across the different cell types and second, we performed gene set enrichment analysis using both KEGG and the MSigDB (GO) database (refer to Materials and Methods).

Compared to mock, CF cultures infected with PAO1 had the fewest DEG, followed by non-CF and BCi-NS1.1 cultures which showed the highest number of DEG. For all CF, non-CF, and BCi-NS1.1 infected samples, we observed mainly upregulated genes (Fig 5B, Table S3). Enrichment analysis showed that *P. aeruginosa* triggers the upregulation of several pathways related to inflammation via NF-kß and TNFα and overexpression of cytokines, including IL-6 and IL-17 signaling (Table S4). Of note, colony-stimulating factor CSF3 and pro-inflammatory cytokine IL17C were among the most DEG across all host cells (mean log_2 FoldChange = 12.01 ± 1.5 and 11.8 ± 0.6, respectively) (Fig 5C). Other highly expressed genes include chemokine ligand 20 (CCL20) and tumor necrosis factor (TNF), Toll-like Receptor (TLR)-2, TLR4 (involved in recognition of bacterial pili or LPS), IL1B, IL6, CXCL8 (involved in first stages of infection) and DEF4BA with antimicrobial capabilities (Fig 5C).

We found that the host responses after infection with the less virulent strain *pscC* showed limited differences compared to PAO1 infection. In fact, only 65 unique genes were differentially expressed (upregulated) in tissues infected with PAO1 relative to *pscC* (Fig 5E). Pathways related to cytokine signaling and immune system response were overrepresented among the set of genes with the highest expression in PAO1-infected non-CF and BCi-NS1.1 cultures (Fig 5F). This suggests that, at the time tested, the delivery of effectors from the T3SS partially affects host cell gene expression. However, *P. aeruginosa* has a wide array of other host-related virulence factors contributing to infection and concomitant inflammatory response, possibly explaining the limited difference between the PAO1 and *pscC* mutant strain.

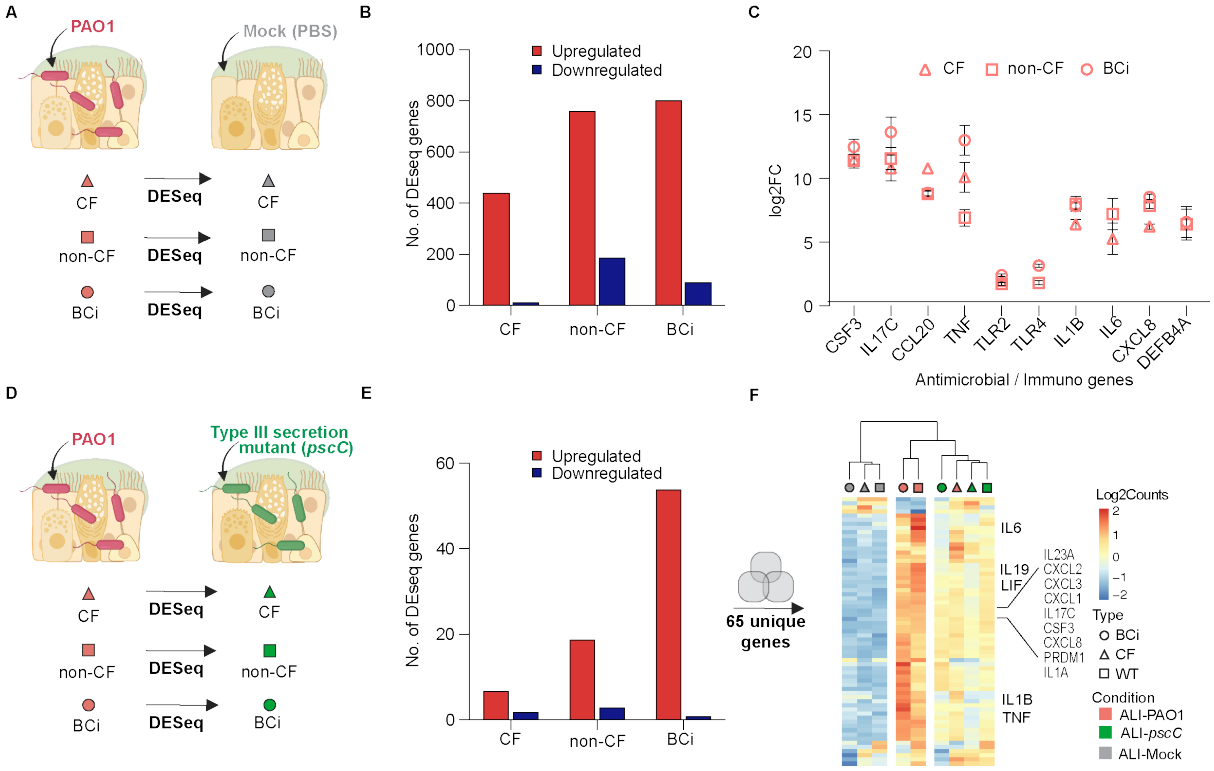

Fig 5. Intrinsic host responses before and after colonization with PAO1. A) Representation of the individual differential expression (DE) comparisons between cultures were performed: PAO1 infected cultures and their mock. B) Number of differentially expressed genes (DEG) shown as upregulated (red) and downregulated (blue). An adj p value < 0.05 and $\log_2$FoldChange > |1| was used as cutoff C) $\log_2$FoldChange of immune genes when comparing PAO1 infected and mock. Only significantly expressed DEG are shown. D) Representation of the DEG comparisons between PAO1-infected and *pscC*-infected cultures. E) Number of DEG

shown as upregulated (red) and downregulated (blue). F) Heatmap of log_2 read counts scaled for each gene (row) from the unique 65 DE genes from D). Each column represents the mean of the three biological replicates sequenced clustered based on the result of pvclust analysis. CF: cystic fibrosis; BCi: BCi-NS1.1.

P. aeruginosa *PAO1 and* pscC *elicit differential response upon interaction with human airway epithelial cells*

The analysis of the bacterial transcriptome aimed to evaluate how the expression profile of PAO1 and *pscC* vary when interacting with different cell types (Fig 6A). As previously shown in Fig 4C, whole-gene expression profile of both bacteria was similar in the non-CF and BCi-NS1.1 models. Indeed, no PAO1 gene was DE when comparing non-CF vs BCi-NS1.1 infections, and a similar observation was obtained for *pscC* with only 3 DEG (Fig 6B top and bottom panel, Table S5). The PAO1 transcriptome showed only 56 and 79 (total analyzed transcriptome n = 4255 genes) DEG in CF vs non-CF and CF vs BCi-NS1.1 infections, respectively, suggesting that PAO1 behaves rather similarly when colonizing different ALI cultures (Fig 6B). In contrast, *pscC* strain showed a 3.9-fold to 5-fold increase in DEG in the CF vs non-CF and CF vs BCi-NS1.1 comparisons, respectively (Fig 6B, bottom panel). This suggests that the activity of T3SS has a direct effect on bacterial expression profile upon infection with CF cultures.

Considering similarities between bacterial gene expression in non-CF and BCi-NS1.1 ALI models, we next focused on the CF vs non-CF comparison and compared the expression profiles of *pscC* and PAO1 (Fig 6B underlined boxes). Deletion of T3SS *pscC* gene elicited a much higher dysregulation of genes (up- or downregulated) when infecting CF ALI cultures (unique DEG = 232, PAO1 specific n= 14, *pscC* specific = 177) (Fig 6B). From the total unique DEG (n = 232), 41 were common to both strains and included upregulation of genes involved in respiration under iron-limiting conditions such as 1) bo_3 quinol oxidase (*cyo*) genes and 2) members of the *fumC-sodM* iron-responsive operon [41,42] (Table S6). Likewise, they both downregulate several pathways reported as involved in virulence, such as the production and transport of phenazines (among others: *phz1* and *phz2* operons), nitrate reductase *nirA,* and fucose-specific lectin *lecB* [43–45].

When comparing CF vs non-CF infections for *pscC*, we found enrichment (upregulated) of mainly 3 categories of genes: 1) iron chelation (related to heme uptake, pyoverdine, and pyochelin transport), 2) sulfate metabolism (*cysAWT-sbp* operon), and 3) lipid A modifications

(Fig 6C, left panel and Table S6). Contrarily, several genes related to virulence including QS and biofilm pathways, were enriched in the downregulated class (Fig 6C, right panel and Table S6). For example: 1) genes from the *pseudomonas* quinolone signal (PQS) cluster, 2) rhamnolipids coding genes, 3) the type 6 secretion system H2 gene cluster (H2-T6SS), 4) genes from oxide-sensing mechanisms, and 5) elastases (*lasB*) and pyocyanin biosynthetic genes. This suggests that upon CF infections, *P. aeruginosa* regulates several pathways involved in iron starvation, respiration, and virulence mechanisms which were previously identified as differentially expressed *in vivo* in CF airways and contribute to the establishment of the infection [46,47].

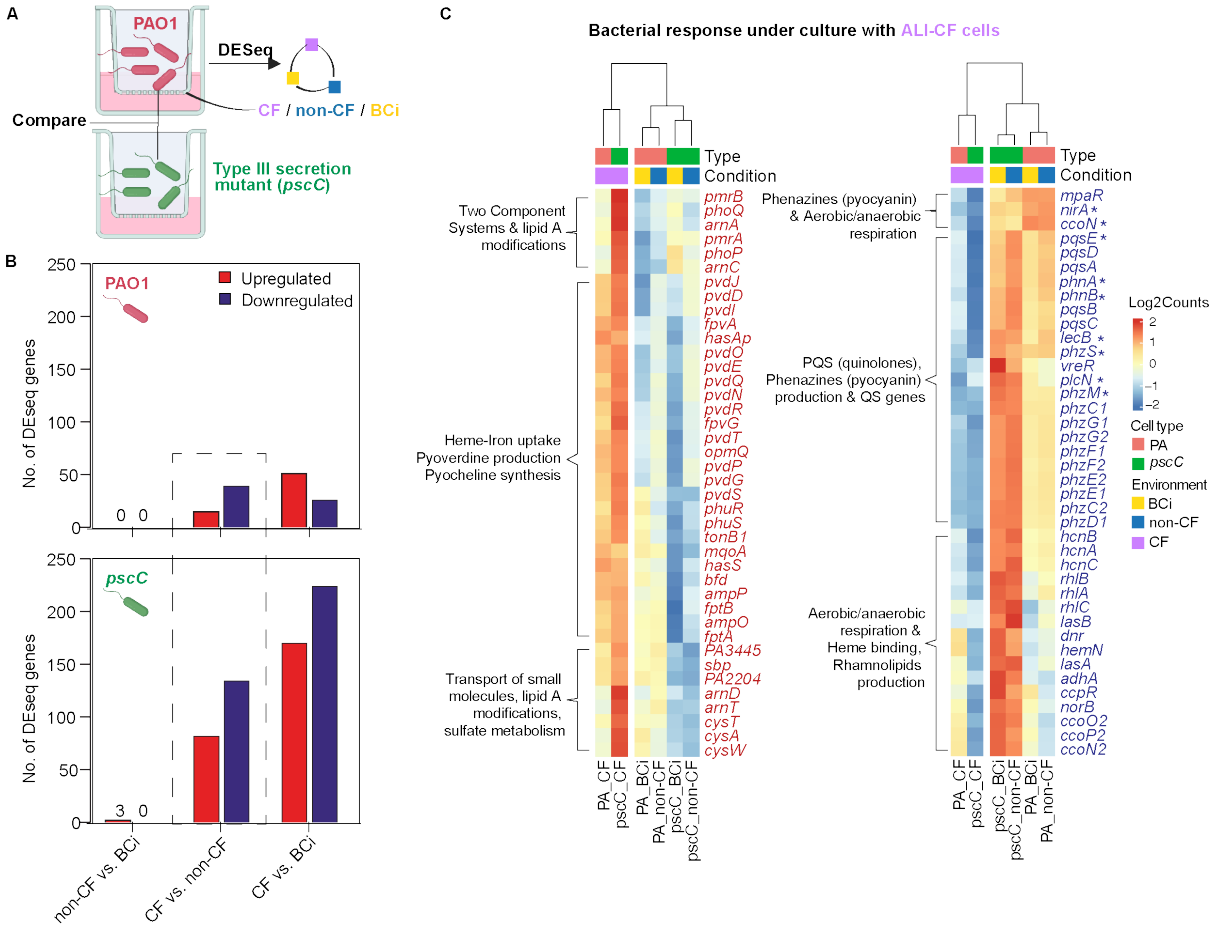

Figure 6. *Pseudomonas aeruginosa* responses upon interaction with different human cell types. A) Representation of the differentially expressed gene (DEG) comparison of PAO1 and *pscC* transcriptomes analyzed in different ALI models, ie. non-CF vs. BCi, CF vs. non-CF, and CF. vs BCi. B) Number of DEG shown as upregulated (red) or downregulated (blue) and separated by strain (PAO1 top and *pscC* bottom panel, respectively). An adj p value < 0.05 and $\log_2$FoldChange > |1| was used as cutoff. C) Heatmap of $\log_2$ read counts scaled for each gene

(row) present in selected categories from Table S6, comparison *pscC* CF vs. non-CF. Each column represents the mean of the three biological replicates sequenced, clustered based on the result of pvclust analysis. Genes with asterisk (*) were differentially expressed (DE) in both PAO1 and *pscC* strains when comparing CF vs. non-CF models. CF: cystic fibrosis; BCi: BCi-NS1.1.

Discussion

Persistent bacterial infections are often associated with antibiotic resistance, but several other underlying mechanisms have been brought forward to explain why antibiotic treatment fails to eradicate the infecting bacteria. Thus, eradication failure of *P. aeruginosa* in pwCF requires the understanding of the infection and colonization process and the interactions between the host and the pathogen. For this, we have established and compared infection model systems based on ALI cultures of different human airway epithelial cells (non-CF, CF and the BCi-NS1.1 cell line), in which we have quantified infection outcomes during the early stages of colonization by different clinical isolates of *P. aeruginosa*.

In a first physiological response investigation of the differentiated airway epithelial ALI cultures, we quantified a number of tissue parameters after the bacterial colonization: epithelial damage (transepithelial electric resistance, TEER), cytotoxicity (release of lactate dehydrogenase, LDH), immune system recruitment (interleukin 8), and bacterial distribution in the tissue (confocal microscopy). Together, the patterns of changes of these 4 parameters provide highly valuable information about the inherent properties of the included tissues, as well as about the virulence of the infecting bacteria. Thus, our investigations revealed that irrespective of the host tissues (non-CF and CF donors or the BCi-NS1.1 cell line), colonization of different epithelia was predominantly driven by the intrinsic bacterial virulence potential. Infection clusters were neither based on the strain's genetic background (that is, isolates from the same lineage were not always grouped together), nor on the level of adaptation (that is, chronic late strains did not always show reduced virulence). Yet, several studies of clinical strains grown *in vitro* have revealed convergence in different lineages to an adapted and low virulent phenotype as chronic infection progresses [21,24,36,37]. However, transcriptomic and proteomic changes do not always positively correlate with *in vivo* data due to differences in growth conditions and the lack of host interactions [46,47]. Importantly, the ALI system used in

this study has the potential to become a powerful infection predictive method, as it allows the evaluation of drug efficacy, immune system activity, host responses, and inter-species interactions, which are fundamental to understanding infection progression and improving treatment outcomes. Recently, certain mutations in *P. aeruginosa* were discovered to be involved in novel adaptive mechanisms that transcend conventional antibiotic resistance, which highlights the need for host-focused approaches to develop more effective strategies for managing bacterial infections [29,30]. Interestingly, in our ALI model system using CF cultures, we observed similar infection profiles of both laboratory and clinical strains of *P. aeruginosa*, whether treated with ETI modulators or not. This is in agreement with recent works showing that, albeit there is a reduction of bacterial load in pwCF treated with ETI modulator, bacteria still persist in the airway [9,11].

Interactions of *P. aeruginosa* with airway epithelial cells grown in ALI systems have recently been investigated by transcriptomic analyses to study the pathogen, the host, or both [31,33,34,48,49]. Given the system's complexity and the technical challenges of working with primary cells ALI infections, we only explored the gene expression response of PAO1 and the less virulent *pscC* strain when infecting ALI models from a CF and a non-CF donor together with the BCi-NS1.1 cell line. Although we cannot rule out differences in gene expression between donors, our ALI infections and non-RNA readouts were carried out with several donors, where infection patterns were evened out. Similar to earlier research, we found that colonization of host epithelium with *P. aeruginosa* triggers the upregulation of NF-kß and TNFα pathways and overexpression of cytokines including those coding for IL-6 and IL-17 signaling [33,34,49]. Moreover, our three ALI models shared the same profile with 368 common DE genes related to bacterial infection response such as inflammatory pathways, response to bacteria and LPS. In agreement with the latter, infections carried out with 8 different donors (n = 3, non-CF and n = 5, CF) showed similar trends in IL-8 secretion for PAO1 across the different cell types. On the other hand, like PAO1, deletion of T3SS also induced host inflammation, and only 65 genes related to cytokines and immune markers (e.g. CSF3, IL1B, IL6, CXCL8 and TNF) were upregulated during PAO1 infection while they were significantly downregulated during the *pscC* infection when comparing PAO1 vs *pscC* infected samples (Fig 5F and Table S5). This correlates well with infection readouts, in which *pscC* strain still showed an intermediate virulence potential between PAO1 and the more adapted clinical strains (Fig 3).

Upon infection and depending on the availability of nutrients and/or signals triggered by host cells, *P. aeruginosa* tightly controls the regulation of a wide array of virulence factors involved in host-mediated respiratory infections [26]. In our CF model, both PAO1 and *pscC* strain limit the expression of *lasB*, a principal extracellular virulence factor, and the biosynthesis of pyocyanin, both contributing to inflammation and epithelial disruption [50]. The downregulation of these genes may enable the bacteria to evade the host's immune system and reduce host inflammation, as observed in our infected CF models, which showed fewer DEG (n = 442) compared to the non-CF (n = 761) and BCi-NS1.1 (n = 804). Strikingly, the response between CF cells and the T3SS-deficient *pscC* strain showed a much more complex dysregulation resembling many of the features already seen in CF clinical isolates. This suggests that CF models would be the best suitable approach when the research focus is on bacterial transcription. Besides phenazine biosynthesis, the *pscC* strain also shows a downregulation of the PQS system and rhamnolipid production, mirroring key features of CF late chronic strains [46]. Another example is the high expression of genes involved in the production and transportation of siderophores pyoverdine (*pvd*) and pyochelin (*pch*), as well as the assimilation of heme (*phu* and *has* systems) [47], which suggests that the accessibility of these micronutrients is limited in CF ALI models relative to non-CF.

While infection model systems allow for a more representative analysis of bacterial phenotypes, they also have some limitations. It was, indeed, surprising that only a few isolates showed significant differences in one or two readouts between CF and non-CF cultures. This result may be due to several factors: a) the model may not accurately reflect the conditions bacteria encounter in the lung (i.e., presence of immune cells, antibiotic treatment, oxygen and micronutrient gradients), b) the length of infection (14 or 38 h) might be sub-optimal for discriminating small infection pattern responses, c) the closed nature of the ALI transwells which limits mucociliary clearance and mucus buildup, potentially making the different cell types similar, or d) the lack of residing airway microbiota which could influence the host-pathogen interaction. Therefore, further investigations are required to evaluate each parameter.

Altogether, we explored the virulence potential of persistent clones of *P. aeruginosa* when colonizing different airway epithelial tissues grown at the ALI interface. We covered a variety of bacterial lineages and host donors and defined clusters of infection properties. Furthermore, we quantified the transcriptional responses of both pathogen and host upon

502 infection at a whole population level. Our data foster the need for studies using host-pathogen
503 models to recapitulate the *in vivo* conditions of pathogenic diseases. Moreover, given the
504 more appropriate physiological environment, it serves as a platform for evaluating treatment
505 efficacy and identifying novel therapies for the treatment of persistent infections. Still, further
506 studies including immune cells, antibiotic treatment, and other infecting species are needed
507 to understanding infection progression, antibiotic treatment failure and new mechanisms of
508 persistence.
509
510

Materials and Methods

Primary human airway cells and cell line used

Nasal brushing, nasal polyps and distal lung biopsies were obtained from pwCF (n = 10) and non-CF control (n = 5) donors. Details of CFTR mutation and sample usage are provided in Table S2. Nasal brushes were obtained using a 2.5mm sterile cytology brush and placed in Dulbecco´s modified essential media (DMEM) supplemented with primocin (1 mg/mL), gentamicin (100 µg/mL) and Amphotericin B (2.5 µg/mL) until further processing for cell culture. Polyps were obtained from patients undergoing endoscopic sinus surgery. Tissue specimens were surgically removed and immediately placed in DMEM supplemented with same antibiotics as brush biopsies. Size of explants obtained was of approximately 20–30 mm^2. Explants were washed three times with fresh, sterile media, to remove blood and mucous when was present.

Isolated basal cells were seeded and expanded in T-25 cm^2 flasks (corning Life Sciences) previously coated with human type I collagen (Gibco, A1048301) in a 37°C, 5% CO2 humidified incubator, using Pneumacult-Ex Plus medium (STEMCELL Technologies, 05040) supplemented with Pneumacult-Ex 50x supplement (STEMCELL Technologies, 05008), 96 ng/mL hydrocortisone (STEMCELL Technologies, 07925), 10 µM Y-27632 ROCK inhibitor (Bio-Techne #1254/10), and the same antibiotics used before. Following expansion, 1.5 x 10^5 cells were seeded onto 6.5-diameter-size transwells with 0.4 µm pore polyester membrane insert (Corning Life Sciences) previously coated with type I collagen.

Once cells reached full confluency, Air-Liquid Interface (ALI) was established, by removing media from the apical chamber and replacing media in the basolateral chamber with Pneumacult-ALI medium (STEMCELL Technologies) supplemented with 480 ng/mL hydrocortisone (STEMCELL Technologies), 4 µg/mL heparin (STEMCELL Technologies, 07980), Pneumacult-ALI 10x supplement (STEMCELL Technologies) and Pneumacult-ALI maintenance supplement (STEMCELL Technologies). ALI cultures were grown at 37 °C and 5% CO_2 in a humidified incubator for 28 days, with media replacement twice a week.

Epithelial polarization was monitored by measurements of the transepithelial electrical resistance (TEER) using an EVOM2 (World Precision Instruments) and a chopstick electrode (STX2; World Precision Instruments). Following 15 days under ALI conditions, the apical surface was washed with 1x Phosphate Buffered Saline (PBS) once a week to remove accumulated mucus. For primary cells only passage 1-3 were used for ALI cultures. Different

studies have show that both human nasal and bronchial airway epithelial cells grown for ALI cultures are representative of lung biology and recreate its physiology [28,51].

The Basal Cell Immortalized Non-Smoker 1.1 (BCi-NS1.1) cell line [35] was used for comparison with the primary ALI infection model systems. BCi-NS1.1 cell expansion, ALI establishment, differentiation and maintenance of cell cultures was performed as described above for primary cells without the addition of antibiotic to media culturing.

Modulator treatment

On day 28, a combined CFTR-modulator treatment of elexacaftor (VX-445, MedChemExpress), tezacaftor (VX-661, Selleck Chemicals LLC) and ivacaftor (VX-770, Selleck Chemicals LLC), was added for 24h to the basolateral medium, with a final concentration of 3 µM, 10 µM and 5 µM in 0.15% dimethyl sulfoxide (DSMO), respectively. The treatment was prepared fresh before each experiment. Controls were treated with similar concentration of DSMO.

Measurement of CFTR function and rescue

Transepithelial electrical conductance (TEEC) is considered a parameter to assess the CFTR function, as demonstrated in previous studies [52–54]. TEEC is calculated from the reciprocal value of TEER measurements:

$$Transepithelial\ electrical\ conductance(TEEC) = \frac{1}{Resistance} = \frac{1}{TEER}$$

$$\Delta TEEC = TEEC(\max) - TEEC(inhib)$$

The rescue of CFTR function through ETI treatment facilitates the transepithelial chloride ion transport, and increases the CFTR-dependent TEEC.

TEER measurements were obtained after maximal stimulation of CFTR channels with forskolin plus genistein and subsequent inhibition with PPQ-102, before converted to TEEC. The difference between maximum activation and inhibition (ΔTEEC) reflects the CFTR activity in the epithelia, and the difference between treated and un-treated cells reflects the partial rescue of CFTR function by ETI. First, Coon's modified Ham's F12 medium (DiagnoCine), where NaHCO3 was replaced with 20 mM Na-Hepes (SigmaAldrich) (pH 7.3), was added to both sides of the cell layer, and after one hour of equilibration, a baseline TEER was measured in each transwell as described previously (workflow is shown in Figure S2). After 10 minutes, apical

amiloride was added to block sodium channels (ENaCs), and to avoid sodium-dependent currents. Apical and basolateral medium was replaced with new solutions containing forskolin 10 µM (TargetMol) and genistein 50 µM (TargetMol) activate CFTR function. To subsequently inhibit CFTR function, a solution containing CFTR inhibitor PPQ-102 30 µM (TargetMol) was added to the apical side. Between each step, a 10 min incubation time was allowed, after which TEER was measured and values were subsequently converted to TEEC. All donors, CF and non-CF, were tested to assess the ETI response, in at least three technical replicates. Following test of CFTR function, the cell cultures were discarded, and were not utilized in subsequent infection experiments.

Clinical strains, growth conditions and fluorescent tagging

Strains used in this study are summarized in Table S1. Clinical strains were obtained from sputum samples from pwCF attending or who have attended the Copenhagen Cystic Fibrosis Center at University Hospital Rigshospitalet, Copenhagen, Denmark. Sputum sampling is a part of the routinary visits to the CF clinic and was not performed for the purpose of this research. All clinical strains except for DK01_E, DK02_E, were previously sequenced and their genomic and transcriptomic profile was characterized [36].

P. aeruginosa reference strains PAO1, PA14 and C-clone were obtained from the Leibniz Institute DSMZ collection with references DSM22644, DSM19882 and DSM29238, respectively. Additionally, an isogenic mutant of PAO1, encoding the *pscC* gene, part of the T3SS, was constructed in the lab.

All strains were tagged with a superior green fluorescent protein (sfGFP) to enable visualization by confocal microscopy. Bacterial strains were GFP-tagged by 4 parental mating using the miniTn7 delivery plasmid with rhaSR-PrhaBAD inducible promoter (pJM220) [55]. Plasmid was engineered in the lab to accommodate sfGFP gene. Transformants were selected on *Pseudomonas* isolation agar supplemented with Gentamicin 30 µg/mL. The final sfGFP-tagged strains were verified by checking green fluorescence using a Leica DM4000 B epifluorescence microscope and confirming normal growth rate (Fig S7).

Phenotypic characterization of *P. aeruginosa* strains

Strains were characterized based on their growth in synthetic cystic fibrosis media (SCFM), bacterial movement and antibiotic susceptibility profiles. Briefly, single colonies were picked

and grown on liquid Luria-Bertani broth (LB) cultures. Cultures were standardized to OD = 0.1 and further diluted to OD = 0.01 in SCFM media and growth was recorded every 15 min for 18 h in a 96 well plate reader at 37°C with continuous shaking. Doubling times and growth rate estimations were calculated using Graph Pad Prism software (v 10.2.2), focusing on the exponential part of the growth curve. For swimming assay, 2 µl of the 0.1 OD cultures were plated on the center of tryptone broth plates (10 g/L tryptone, 5 g/L NaCl) with 0.25 % of agarose. Motility diameter was measured after incubation for 6 h at 37°C and additional 16 h at room temperature. For antimicrobial susceptibility, the microdilution method from EUCAST was used (The European Committee on Antimicrobial Susceptibility Testing 2023). Cultures were standardized to Mc Farland (5 x 10^5 CFU/ml) and grown in Müller-Hinton broth with serial fold dilutions of either tobramycin, ceftazidime, or ciprofloxacin for 16 h in 96 well plates at 37 °C with shaking conditions. MIC was calculated as the concentration of antimicrobial that completely inhibited the growth of the strain as detected by the naked eye. All phenotypic experiments were performed with 3 independent cultures.

Infection of ALI cultures with *P. aeruginosa* strains

Overnight of *P. aeruginosa* cultures were standardized to OD = 0.05 (fast growers) – 0.1 (slow growers) and grown until mid-exponential phase in 5 mL of LB medium. Subsequently, 1 mL of culture was centrifuged at 5000 × g for 5 min, and bacterial pellets were washed with PBS and resuspended in PBS at a concentration of 10^5 CFUs/mL. For each strain, the relationship between OD and CFU count was tested in triplicates to achieve reproducible results. 10 µL aliquot of this solution, containing 10^3 CFUs, was inoculated onto the apical side of fully differentiated ALI cultures, each with 600 µL of supplemented Pneumacult-ALI maintenance medium in the basolateral chamber. Non infected controls were inoculated with an equal volume of bacteria-free PBS. Infected cells were incubated at 37 °C and 5% CO2 in a humidified incubator for the specified duration required to characterize the infection (14 h for fast growers and 38 h for slow growers). Following infection time, 200 µL of PBS was added to the apical side, and TEER was measured.

Subsequently, the 200 µL of PBS from the apical side and 600 µL of medium from the basolateral side were collected and CFUs present in these samples were quantified by plating 10 µL of serial dilutions on LB-agar plates. The remaining samples were preserved at −80 °C for future analysis. For quantification of bacterial CFUs attached to the epithelium 200 µL of

638 0,01% triton in PBS was added to the apical part, and the epithelial layer was disrupted using
639 a cell scraper. CFUs present in the suspension were determined as explained above.
640
641 **Immunofluorescence staining and confocal microscopy**
642 ALI cultures were fixed with 4% paraformaldehyde added in both apical and basolateral
643 compartments for 20 min at 4 °C. After fixation, cells were washed 3 times with PBS after
644 which and incubation of 1 h at room temperature (RT) with blocking buffer (0.1% Triton X-100,
645 1% saponin, 3%BSA in PBS) was performed to allow permeabilization. Then, whole transwells
646 were stained overnight with a 100 µL solution of MUC5AC (mouse monoclonal, Invitrogen) at
647 1:100 dilution. For CFTR staining, a solution of anti-CFTR 570 at 1:100 dilution and incubated
648 overnight at 4°C was used. The following day, a second staining was performed with a new
649 100 µL aliquot containing Phalloidin-Alexa Fluor 555 (Invitrogen), DAPI (Thermo Scientific) and
650 Alexa Fluor 647 (Invitrogen) at 1:400, 1:750, 1:500 dilution, respectively. All stainings were
651 conducted in a buffer containing 3%BSA and 1% saponin in PBS. After staining the membranes
652 were removed from their supports with a scalpel and mounted on glass slides with
653 VECTASHIELD® Antifade Mounting Medium (VWR). Images were acquired with a Leica Stellaris
654 8 Confocal Microscope (40× magnification, 1.3 oil) and analyzed using the LasX software
655 1.4.4.26810 (Leica).
656
657 **Lactate dehydrogenase (LDH) release and Human IL-8 production**
658 Aliquots from basolateral compartment were further used for measuring LDH and IL-8 release
659 following the manufacturer's instructions of the Invitrogen™ CyQUANT™ LDH Cytotoxicity
660 Assay Kit (Invitrogen, C20301) and Human IL-8/CXCL8 DuoSet ELISA kit (Bio-Techne, DY208).
661 LDH was measured using 50 µL of media and measuring absorbance at 680 nm and 490 nm.
662 For IL-8 quantification, basolateral media was diluted to 1:10 and absorbance was measured
663 at 450nm and 540nm. All individual ALI infected samples were tested in triplicates.
664
665 **RNA extraction from ALI cultures and sequencing library preparation**
666 Lung biopsy from one wild-type donor (non-CF 16) and nasal brush from one pwCF (CF14) and
667 the BCi-NS1.1 cell line were used to perform infection models with PAO1 and *pscC* strains, in
668 triplicates. ALI models and infections were performed as for the rest of the infections in this

work. Compared to other donors, infection readouts were within the experimental variability (Table S2).

Extraction of RNA was performed using the Qiagen RNeasy Plus Mini kit and following manufacturing protocol. Briefly, after infection was performed and TEER was measured, PBS media was removed from the top and 300ul of RNA protect Cell Reagent was added. Adherent cells detached after thorough pipetting without need of trypsin. Two transwells were collected within 300ul of sample and froze at -80 until RNA extraction. For enzymatic lysis, samples were thawed and centrifuged to remove RNA protect, and then 1ml RNA-se free water containing 1 mg/ml of lysozyme was added and incubate for 30min at 37°C. Then samples were centrifuged and resuspended in 600ul RLT Buffer (with ß-mercapto) and follow Qiagen protocol to recover RNA fragments over 200 nt. Recovered RNA was quantified using fluorimetric quantitation with Qubit® RNA BR Assay kit (Invitrogen) and RNA integrity was measured on an Agilent Bioanalyzer 2100 machine (Agilent technologies) using a RNA Nano kit. All samples had a percentage of RNA fragments > 200 nt (DV_{200}) ranging between 50%-75% and were further processed. 2 µg of eluted RNA was treated with DNAse I (Invitrogen) for 30min at 37°C in a final volume of 50µl. Further clean up with Qiagen columns was performed by mixing 3 times RLT Buffer (without ß-mercapto), with 3 times 95-100% ethanol and 1 time sample (50µl sample + 150µl RLT + 150µl EtOH). Following 2 wash steps with RPE, RNA samples were resuspended in 20-25 µl RNA-se free water. 500 ng of RNA was used as template to prepare sequencing libraries with Illumina Stranded Total RNA Prep with Ribo-Zero Plus kit (Illumina). Sequencing was performed on an Illumina NextSeq 500 sequencer, using a high output kit, generating a minimum of 30 million reads per sample (75 bp, single end reads).

As it has been shown that bacterial transcripts represent only a fraction of total RNA within host cells [56], we extracted RNA from two independent infected transwells and consider it as one replica, so the total of infections per condition was 6, and only a max. of 12 samples were pooled for sequencing run. This strategy enables an increased yield in the bacterial RNA in the infected cultures ranging from 2.5M to 10M reads depending on the bacteria and cell type (Fig S8, Table S7). For *pscC* infected samples (BCi-*pscC* 1-3, CF-*pscC* 2-3, non-CF-*pscC* 1-3) a second round of sequencing was done to reach a minimum cutoff of 1M reads for *Pseudomonas* genome. Table S7 contains the sequencing reads achieved for both runs (BCi-*pscC* 1a and BCi-*pscC* 1b, etc.).

Host-Microbe transcriptome analysis

Sequencing reads were analyzed with our in-house pipeline updated for host-microbe samples [57]. Briefly, low-quality bases and contaminant adapters were trimmed using Trimmomatic (v 0.35), discarding reads shorter than 35 nt. Reads were further processed using the SortMeRNA tool (v 2.1) to remove reads generated from residual rRNA transcripts. High-quality human and bacterial reads were separated in silico by mapping reads using the BWA aligner and MEM algorithm against the human genome assembly GRCh38.p9 retrieved from the NCBI database. Reads not mapping on the human genome were used as input for analyzing the transcriptionally active *P. aeruginosa* population mapping against *P. aeruginosa* PAO1 genome (NCBI: NC_002516.2) using BWA (0.7.15-r1140) aligner and MEM algorithm with default parameters.

Gene expression analysis

For gene expression analysis, mapped reads deriving from host and *P. aeruginosa* were counted using htseq-count (v 0.7.2). Count tables were then imported into R for differential gene expression (DEG) analyses. Host read counts were pre-filtered based on >= 10 reads counts per condition (sum of replicates), yielding a count data of 18746 genes. Then, counts were normalized using variance stabilizing transformation (VST-normalization) on all samples together in the R package DESEq2 (v 1.44.0) with option blind = TRUE [58]. A similar approach was set for bacterial reads, counts were pre-filtered based on all replicate's samples having >= 10 reads, reaching a count data of 4255 *P. aeruginosa* genes. Normalized counts were used to evaluate whole transcriptome similarities between replicates and conditions using principal component analysis (PCA) and hierarchical clustering analysis (HCA). PCA was performed using plotPCA() function and visualize with ggplot(). When needed, normalized counts of specific set of genes were visualized as heatmaps using pheatmap() function calculating first the replicates mean in each condition.

To get list of log_2FoldChange values, from the initial DESeq2 result table, pair comparisons of specific conditions were extracted using the "contrast" argument from the result() function in DESeq2. For both host and bacteria, DEG were considered statistically significant when log_2FoldChange ≥ |1.0| and an adjusted p value ≤0.05. Significant host DEG were used as input for inspection of gene set enrichment analyses which considers both gene name and

log_2FoldChange values. The "human hallmark set" collection from Molecular Signature Database (MsigDB) which is a non-redudant curated gene set based on GO terms pathways, maintained by the GSEA team (www.msigdb.org) was used in R using functions msigdbr() to call the gene set, and GSEA() for enrichment purposes, with the following parameters: minGSSize=5, maxGSSize=500, pvalueCutoff=0.05, pAdjustMethod=BH. Functional enrichment with the KEGG database using gseKEGG() function, was also performed. Here terms were filtered based on pathway correlation with our infection model. When similar pathways were called (response to lipid vs cellular response to lipid), the one with the smallest padj value was used. Similarly, functional class enrichment in significant bacteria DEG was performed using log2FoldChange values and gene associations with terms present in COGs and KEGG classification databases, using PAO1 annotations from Pseudomonas.com and using it as terms for GSEA(). For gseKEGG() the following parameters were used: organism="pae", minGSSize=5, maxGSSize=500, pvalueCutoff=0.05, pAdjustMethod=BH.

To identify similarities across different DEG lists, UpSet plots were drawn using the UpSet() function from R.

Ethical approval and consent to participate

This study was approved by the local ethics committee of the Capital Region of Denmark (Region Hovedstaden), registration number H-20024750. All patients provided informed consent to participate in the study and for the publication of associated results and pertinent clinical data. Pseudonymization of patient information was performed to sever any links that could lead to patient identification.

Data sharing

Raw sequence data supporting the results of this work are available as SRA BioProject under Accesion No. PRJNA1153754 and accession numbers from individual BioSamples and sequences is summarized in Table S7.

Author Contribution Statement

Claudia Antonella Colque: Methodology, Formal analysis, Investigation, Data curation, Visualization, Writing – original draft, Writing – review & editing. **Signe Lolle:** Methodology, Formal analysis, Investigation, Writing – review & editing. **Ruggero La Rosa:** Formal analysis,

765 Data curation, Visualization, Writing – original draft, Writing – review & editing. **Maria Pals**
766 **Bendixen:** Investigation, Writing – review & editing. **Filipa Bica Simões:** Methodology, Formal
767 analysis, Investigation, Writing – original draft, Writing – review & editing. **Kasper Aanæs**:
768 Resources. **Søren Molin:** Conceptualization, Supervision, Writing – review & editing. **Helle**
769 **Krogh Johansen:** Conceptualization, Funding acquisition, Resources, Supervision, Writing –
770 review & editing.
771
772 **Acknowledgments**
773 The authors thank the Danish pwCF and the non-CF donors who participated in this study,
774 Laura Elisabeth Bojesen Haapalo and Rene Horsleben Petersen (Department of Cardiothoracic
775 Surgery, Copenhagen University Hospital, Rigshospitalet, Denmark) for providing and assisting
776 with lung tissue samples, and the nurses from Rigshospitalet CF clinic assisting with patient
777 recruitment and sample collection. We thank the cystic fibrosis foundation (CFF) for providing
778 the CFTR anti570 antibody, and Ronald G. Cristal (Weil Cornell Medical College, New York,
779 USA) for providing the BCi-NS1.1 cell line. This research was funded by a Challenge Grant (Ref.
780 nr.: NNF19OC0056411) and a grant from The John and Birthe Meyer Foundation awarded to
781 HKJ. HKJ and SM were supported by a grant from CAG. - Greater Copenhagen Health - Science
782 – Partners (GCHSP), 2020. We thank the Infection Microbiology group (Asha Maria Rudjord
783 Levann, Oihane Irazoqui Sanchez, Pablo Laborda Martínez, Janus Anders Juul Haagensen) for
784 their insightful comments and discussions. We thank Elio Rossi (Department of Biosciences,
785 University of Milan) for his advice on transcriptomics analysis, and Nicoletta Pedemonte from
786 IRCCS Institute Gaslini, Genova for her assistance in modulator treatment assays.
787

788 **References**

789

790 1. La Rosa, R., Johansen, H. K. & Molin, S. Persistent Bacterial Infections, Antibiotic
791 Treatment Failure, and Microbial Adaptive Evolution. *Antibiotics* **11**, 419 (2022).
792 2. Haney, E. F. & Hancock, R. E. W. Addressing Antibiotic Failure—Beyond Genetically
793 Encoded Antimicrobial Resistance. *Front. Drug. Discov.* **2**, 892975 (2022).
794 3. Sheppard, D. N. & Welsh, M. J. Structure and Function of the CFTR Chloride
795 Channel. *Physiological Reviews* **79**, S23–S45 (1999).
796 4. O'Sullivan, B. P. & Freedman, S. D. Cystic fibrosis. *The Lancet* **373**, 1891–1904
797 (2009).
798 5. Douglas, T. A. *et al.* Acquisition and eradication of P. aeruginosa in young children
799 with cystic fibrosis. *European Respiratory Journal* **33**, 305–311 (2008).
800 6. Rosenfeld, M. *et al.* Diagnostic accuracy of oropharyngeal cultures in infants and
801 young children with cystic fibrosis. *Pediatr. Pulmonol.* **28**, 321–328 (1999).
802 7. Heijerman, H. G. M. *et al.* Efficacy and safety of the elexacaftor plus tezacaftor plus
803 ivacaftor combination regimen in people with cystic fibrosis homozygous for the
804 F508del mutation: a double-blind, randomised, phase 3 trial. *The Lancet* **394**, 1940–
805 1948 (2019).
806 8. Szabo, M. M. *et al.* Impact of elexacaftor/tezacaftor/ivacaftor on respiratory
807 colonization in an adult cystic fibrosis clinic. *The American Journal of the Medical*
808 *Sciences* **367**, 337–342 (2024).
809 9. Armbruster, C. R. *et al.* Persistence and evolution of *Pseudomonas aeruginosa*
810 following initiation of highly effective modulator therapy in cystic fibrosis. *mBio* **15**,
811 e00519-24 (2024).

10. Ledger, E. L. *et al.* Impact of CFTR Modulation on *Pseudomonas aeruginosa* Infection in People With Cystic Fibrosis. *The Journal of Infectious Diseases* **230**, e536–e547 (2024).
11. Nichols, D. P. *et al.* Pharmacologic improvement of CFTR function rapidly decreases sputum pathogen density, but lung infections generally persist. *Journal of Clinical Investigation* **133**, e167957 (2023).
12. Bartell, J. A. *et al.* Omics-based tracking of *Pseudomonas aeruginosa* persistence in "eradicated" cystic fibrosis patients. *Eur Respir J* **57**, 2000512 (2021).
13. Mésinèle, J. *et al.* Risk factors for Pseudomonas aeruginosa airway infection and lung function decline in children with cystic fibrosis. *Journal of Cystic Fibrosis* **21**, 45–51 (2022).
14. Gellatly, S. L. & Hancock, R. E. W. *Pseudomonas aeruginosa* : new insights into pathogenesis and host defenses. *Pathogens Disease* **67**, 159–173 (2013).
15. La Rosa, R., Johansen, H. K. & Molin, S. Adapting to the Airways: Metabolic Requirements of Pseudomonas aeruginosa during the Infection of Cystic Fibrosis Patients. *Metabolites* **9**, 234 (2019).
16. Pedersen, B. H. *et al.* Metabolic specialization drives reduced pathogenicity in Pseudomonas aeruginosa isolates from cystic fibrosis patients. *PLoS Biol* **22**, e3002781 (2024).
17. Rossi, E. *et al.* Pseudomonas aeruginosa adaptation and evolution in patients with cystic fibrosis. *Nat Rev Microbiol* **19**, 331–342 (2021).
18. Cramer, N. *et al.* Microevolution of the major common *Pseudomonas aeruginosa* clones C and PA14 in cystic fibrosis lungs. *Environmental Microbiology* **13**, 1690–1704 (2011).

19. Fischer, S., Dethlefsen, S., Klockgether, J. & Tümmler, B. Phenotypic and Genomic Comparison of the Two Most Common ExoU-Positive Pseudomonas aeruginosa Clones, PA14 and ST235. *mSystems* **5**, e01007-20 (2020).

20. Jelsbak, L. *et al.* Molecular Epidemiology and Dynamics of *Pseudomonas aeruginosa* Populations in Lungs of Cystic Fibrosis Patients. *Infect Immun* **75**, 2214–2224 (2007).

21. Markussen, T. *et al.* Environmental Heterogeneity Drives Within-Host Diversification and Evolution of Pseudomonas aeruginosa. *mBio* **5**, e01592-14 (2014).

22. Romling, U., Kader, A., Sriramulu, D. D., Simm, R. & Kronvall, G. Worldwide distribution of Pseudomonas aeruginosa clone C strains in the aquatic environment and cystic fibrosis patients. *Environ Microbiol* **7**, 1029–1038 (2005).

23. Weimann, A. *et al.* Evolution and host-specific adaptation of *Pseudomonas aeruginosa*. *Science* **385**, eadi0908 (2024).

24. Yang, L. *et al.* Evolutionary dynamics of bacteria in a human host environment. *Proc. Natl. Acad. Sci. U.S.A.* **108**, 7481–7486 (2011).

25. Bjarnsholt, T. *et al.* The importance of understanding the infectious microenvironment. *The Lancet Infectious Diseases* **22**, e88–e92 (2022).

26. Muggeo, A., Coraux, C. & Guillard, T. Current concepts on Pseudomonas aeruginosa interaction with human airway epithelium. *PLoS Pathog* **19**, e1011221 (2023).

27. Prytherch, Z. *et al.* Tissue-Specific Stem Cell Differentiation in an in vitro Airway Model. *Macromolecular Bioscience* **11**, 1467–1477 (2011).

28. Silva, S., Bicker, J., Falcão, A. & Fortuna, A. Air-liquid interface (ALI) impact on different respiratory cell cultures. *European Journal of Pharmaceutics and Biopharmaceutics* **184**, 62–82 (2023).

29. Goltermann, L. *et al.* Macrolide resistance through uL4 and uL22 ribosomal mutations in Pseudomonas aeruginosa. *Nat Commun* **15**, 8906 (2024).

30. Laborda, P. *et al.* Mutations in the efflux pump regulator MexZ shift tissue colonization by Pseudomonas aeruginosa to a state of antibiotic tolerance. *Nat Commun* **15**, 2584 (2024).

31. Lewin, G. R. *et al.* Application of a quantitative framework to improve the accuracy of a bacterial infection model. *Proc. Natl. Acad. Sci. U.S.A.* **120**, e2221542120 (2023).

32. Swart, A. L. *et al.* Pseudomonas aeruginosa breaches respiratory epithelia through goblet cell invasion in a microtissue model. *Nat Microbiol* **9**, 1725–1737 (2024).

33. Tang, M. *et al.* Evaluating Bacterial Pathogenesis Using a Model of Human Airway Organoids Infected with Pseudomonas aeruginosa Biofilms. *Microbiol Spectr* **10**, e02408-22 (2022).

34. Pleguezuelos-Manzano, C. *et al.* Dual RNA sequencing of a co-culture model of Pseudomonas aeruginosa and human 2D upper airway organoids. *Sci Rep* **15**, 2222 (2025).

35. Walters, M. S. *et al.* Generation of a human airway epithelium derived basal cell line with multipotent differentiation capacity. *Respir Res* **14**, 135 (2013).

36. Espaillat, A. *et al.* Adaptive Evolution of *Pseudomonas aeruginosa* in Human Airways Shows Phenotypic Convergence Despite Diverse Patterns of Genomic Changes. *Molecular Biology and Evolution* **41**, msae022 (2024).

37. Marvig, R. L., Sommer, L. M., Molin, S. & Johansen, H. K. Convergent evolution and adaptation of Pseudomonas aeruginosa within patients with cystic fibrosis. *Nat Genet* **47**, 57–64 (2015).

884 38. Balasubramanian, D., Schneper, L., Kumari, H. & Mathee, K. A dynamic and intricate
885 regulatory network determines Pseudomonas aeruginosa virulence. *Nucleic Acids*
886 *Research* **41**, 1–20 (2013).
887 39. Brencic, A. & Lory, S. Determination of the regulon and identification of novel mRNA
888 targets of *Pseudomonas aeruginosa* RsmA. *Molecular Microbiology* **72**, 612–632
889 (2009).
890 40. Moradali, M. F., Ghods, S. & Rehm, B. H. A. Pseudomonas aeruginosa Lifestyle: A
891 Paradigm for Adaptation, Survival, and Persistence. *Front. Cell. Infect. Microbiol.* **7**,
892 (2017).
893 41. Polack, B., Dacheux, D., Delic-Attree, I., Toussaint, B. & Vignais, P. M.
894 ThePseudomonas aeruginosa fumcandsodaGenes Belong to an Iron-Responsive
895 Operon. *Biochemical and Biophysical Research Communications* **226**, 555–560
896 (1996).
897 42. Arai, H. Regulation and Function of Versatile Aerobic and Anaerobic Respiratory
898 Metabolism in Pseudomonas aeruginosa. *Front. Microbio.* **2**, (2011).
899 43. Shao, X. *et al.* The transcriptional regulators of virulence for Pseudomonas
900 aeruginosa: Therapeutic opportunity and preventive potential of its clinical
901 infections. *Genes & Diseases* **10**, 2049–2063 (2023).
902 44. Fenn, S. *et al.* NirA Is an Alternative Nitrite Reductase from Pseudomonas
903 aeruginosa with Potential as an Antivirulence Target. *mBio* **12**, e00207-21 (2021).
904 45. Thuenauer, R. *et al.* The Pseudomonas aeruginosa Lectin LecB Causes Integrin
905 Internalization and Inhibits Epithelial Wound Healing. *mBio* **11**, e03260-19 (2020).

906 46. Camus, L., Vandenesch, F. & Moreau, K. From genotype to phenotype: adaptations
907 of Pseudomonas aeruginosa to the cystic fibrosis environment. *Microbial Genomics*
908 **7**, (2021).
909 47. Rossi, E., Falcone, M., Molin, S. & Johansen, H. K. High-resolution in situ
910 transcriptomics of Pseudomonas aeruginosa unveils genotype independent patho-
911 phenotypes in cystic fibrosis lungs. *Nat Commun* **9**, 3459 (2018).
912 48. Losol, P. *et al.* Bronchial epithelial cells release inflammatory markers linked to
913 airway inflammation and remodeling in response to TLR5 ligand flagellin. *World*
914 *Allergy Organization Journal* **16**, 100786 (2023).
915 49. Tseng, J., Do, J., Widdicombe, J. H. & Machen, T. E. Innate immune responses of
916 human tracheal epithelium to Pseudomonas aeruginosa flagellin, TNF-α, and IL-1β.
917 *American Journal of Physiology-Cell Physiology* **290**, C678–C690 (2006).
918 50. Jurado-Martín, I., Sainz-Mejías, M. & McClean, S. Pseudomonas aeruginosa: An
919 Audacious Pathogen with an Adaptable Arsenal of Virulence Factors. *IJMS* **22**, 3128
920 (2021).
921 51. Roberts, N., Al Mubarak, R., Francisco, D., Kraft, M. & Chu, H. W. Comparison of
922 paired human nasal and bronchial airway epithelial cell responses to rhinovirus
923 infection and IL-13 treatment. *Clinical & Translational Med* **7**, e13 (2018).
924 52. Pesce, E. *et al.* The Autophagy Inhibitor Spautin-1 Antagonizes Rescue of Mutant
925 CFTR Through an Autophagy-Independent and USP13-Mediated Mechanism. *Front.*
926 *Pharmacol.* **9**, 1464 (2018).
927 53. Pedemonte, N. *et al.* Discovery of a picomolar potency pharmacological corrector of
928 the mutant CFTR chloride channel. *Sci. Adv.* **6**, eaay9669 (2020).

929 54. Gianotti, A., Delpiano, L. & Caci, E. In vitro Methods for the Development and
930 Analysis of Human Primary Airway Epithelia. *Front. Pharmacol.* **9**, 1176 (2018).
931 55. Meisner, J. & Goldberg, J. B. The Escherichia coli *rhaSR-PrhaBAD* Inducible Promoter
932 System Allows Tightly Controlled Gene Expression over a Wide Range in
933 Pseudomonas aeruginosa. *Appl Environ Microbiol* **82**, 6715–6727 (2016).
934 56. Westermann, A. J., Gorski, S. A. & Vogel, J. Dual RNA-seq of pathogen and host. *Nat*
935 *Rev Microbiol* **10**, 618–630 (2012).
936 57. Rossi, E. *et al*. Widespread alterations in systemic immune profile are linked to lung
937 function heterogeneity and airway microbes in cystic fibrosis. *Journal of Cystic*
938 *Fibrosis* **23**, 885–895 (2024).
939 58. Love, M. I., Huber, W. & Anders, S. Moderated estimation of fold change and
940 dispersion for RNA-seq data with DESeq2. *Genome Biol* **15**, 550 (2014).
941
942
943